Dynamic Properties of Low and Moderate Molecular Weight Polystyrenes at Infinite Dilution

S. Amelar, C. E. Eastman, R. L. Morris,† M. A. Smeltzly,‡ and T. P. Lodge*

Department of Chemistry and Department of Chemical Engineering and Materials Science, University of Minnesota, Minneapolis, Minnesota 55455

E. D. von Meerwall

Department of Physics and Institute for Polymer Science, University of Akron, Akron, Ohio 44325

Received August 29, 1990; Revised Manuscript Received February 6, 1991

ABSTRACT: Oscillatory flow birefringence (OFB) has been used to determine the dilute solution and infinite dilution conformational dynamics properties of four low molecular weight polystyrenes (PS) ($M = 2.0 \times 10^3$, 5.5×10^3, 2.0×10^4, and 3.2×10^4) in Aroclor 1248. These results are well-described by the bead–spring model (BSM) of Rouse and Zimm, using exact eigenvalue calculations and small values of the number of subchains, N. The initial concentration dependence of the relaxation times is in good agreement with the extension of Muthukumar and Freed. These results are predicated on the appropriate subtraction of the solvent contribution to the measured solution properties, which, in contrast to the conventional approach, is not given by the volume-fraction-weighted neat solvent birefringence. Additionally, pulsed-field-gradient NMR and forced Rayleigh scattering have been used to determine the infinite dilution diffusion coefficients for five PS samples ($M = 2.0 \times 10^3$, 5.5×10^3, 9.0×10^3, 3.2×10^4, and 9.0×10^4) in the same solvent. These results are well-represented by the Kirkwood–Riseman expression, using the same parameter values as used to interpret the OFB results. Furthermore, the diffusivities are equivalent to those reported for PS in toluene and cyclohexane, when scaled by the respective solvent viscosities. The OFB and diffusivity results have been combined with other literature data for PS in Aroclor 1248, including intrinsic viscosity, radius of gyration, and OFB properties for other molecular weights, to provide a stringent test of the BSM. All of the dynamic properties can be described quantitatively with one set of parameter values. This apparent success of the BSM is surprising, given the simplified description of the chain dynamics at the segmental level and the relatively low molecular weight samples examined. In particular, the OFB data suggest a distinct high-frequency end to the relaxation spectrum, corresponding to the relaxation of a ca. 50 monomer subchain.

Introduction

The conformational dynamics properties of flexible chains in solution can provide critical tests of molecular models in addition to unique characterization information. The former assertion rests on the precise experimental determination of the infinite dilution relaxation behavior, over a wide range of frequency. Measurements of the dynamic shear viscosity, η^* (or the dynamic shear modulus, G^*) and the dynamic shear birefringence, S^*, have been shown to supply such information.[1-16] The frequency-dependent properties reflect characteristic motions over a range of length scales and may therefore be quite sensitive to details in the formulation of any given model. On the other hand, some experimentally more accessible quantities, namely, the radius of gyration, R_g, the translational diffusion coefficient, D_o, and the intrinsic viscosity, $[\eta]$, may be viewed as yielding information on one moment of the monomer distribution function, i.e., predominantly on one length scale. From a characterization perspective, the frequency-dependent properties have also been demonstrated to be particularly dependent on the length and topological arrangement of long-chain branches,[17-20] as well as the location and length of the blocks in block copolymers.[21-23]

A conformational dynamics experiment can be used to measure the longest relaxation time, τ_1, in addition to the relaxation time spectrum, $\{\tau_k\}_{k=1,2,...,N}$; in combination with R_g, D_o, and $[\eta]$, there are at least five independent observables that may be compared with theory. The most extensively employed model for describing the behavior of dilute solutions of flexible polymers, the bead–spring model (BSM) pioneered by Rouse and Zimm,[24] requires specification (in its simplest form) of only three parameters; thus, a stringent experimental test of the model may be performed by determining the molecular weight (M) dependence of these five observables, at infinite dilution. Surprisingly, perhaps, such an extensive examination has apparently not previously been reported for one polymer/solvent system. The primary difficulty lies in determining $\{\tau_k\}$ over a sufficiently wide frequency range. To this end, very viscous solvents and time–temperature superposition have customarily been employed to assess the conformational dynamics via either birefringence or viscoelastic (VE) methods; the system polystyrene (PS)/Aroclor 1248 (A1248) has been investigated the most extensively. However, this polymer/solvent pair is virtually isorefractive, thereby preventing the determination of R_g and D_o by light scattering techniques.

Previously, small-angle neutron scattering has been used to measure R_g for perdeuterio-PS with M between 10^4 and 10^5 in A1248.[25] In this work, we report measurements of the oscillatory flow birefringence (OFB) properties of A1248 solutions of four low and moderate molecular weight PS samples. The data have been extrapolated to infinite dilution and interpreted in terms of τ_1 and $\{\tau_k\}$. In addition, pulsed-field-gradient NMR and forced Rayleigh scattering have been used to evaluate D_o for PS in A1248, over the same range of M as R_g. These results are combined with $[\eta]$ values in the literature,[26] as well as previously reported OFB properties for other PS samples in A1248,[4,14] to provide a more rigorous test of the BSM.

† Current address: Diametrics, Inc., Roseville, MN 55113.
‡ Current address: 3M Co., 3M Center, St. Paul, MN 55144.

0024-9297/91/2224-3505$02.50/0

Table I
Polystyrene Specifications

$M \times 10^{-4}$	M_w/M_n	source
0.2	1.06	Pressure Chemical 61222
0.55	1.1	Goodyear CDS-S-10
0.90	1.06	Pressure Chemical 80314
2.0	1.06	Pressure Chemical 41220
3.2	1.06	Pressure Chemical 80317
9.0	1.04	Pressure Chemical 50522

One important conclusion that may be drawn from extensive VE and OFB measurements on PS/A1248 solutions, as well as from measurements on other chemical systems, is that the correct extraction of the polymer contribution from the measured solution properties is not necessarily simple. Previously, it was assumed that the solvent contribution could be taken as the neat solvent value, i.e., the solvent viscosity, η_s, in the case of η^* measurements, and the volume-fraction-weighted solvent birefringence, $\phi_s S_s$, in the OFB case. However, this is no longer viewed as an appropriate method of extraction; a more reliable procedure is to subtract the experimentally determined high-frequency plateau value of the appropriate loss component, i.e., η_∞' in place of η_s and S_∞' in place of $\phi_s S_s$.[1,3,7-14,16,22] This procedure in general, and the determination of S_∞' in particular, are also discussed in some detail.

Experimental Section

Samples and Solutions. The molecular weights (M), polydispersities, and sources of the six polystyrene (PS) samples employed are listed in Table I. The four samples examined by oscillatory flow birefringence ($M = 2.0 \times 10^3$, 5.5×10^3, 2.0×10^4, and 3.2×10^4) were reprecipitated and freeze-dried prior to use. The concentrations of the solutions used were as follows: 0.0250, 0.0499, 0.0999, 0.148, and 0.200 g/mL for $M = 2.0 \times 10^3$; 0.0175, 0.0350, 0.0526, 0.0700, and 0.0882 g/mL for $M = 5.5 \times 10^3$; 0.0200, 0.0390, 0.0589, 0.0784, and 0.100 g/mL for $M = 2.0 \times 10^4$; 0.0200, 0.0395, 0.0600, 0.0799, and 0.104 g/mL for $M = 3.2 \times 10^4$. NMR measurements were performed on three of these samples, as well as on the $M = 9.0 \times 10^3$ PS, which was used as received. Forced Rayleigh scattering measurements were performed on the samples with $M = 9.0 \times 10^3$, 3.2×10^4, and 9.0×10^4. These three samples were labeled with the photochromic dye 4-(*N*,*N*-dimethylamino)-azobenzene-4'-isothiocyanate (Pierce Chemical Co.). The attachment procedure was essentially that described by Kim et al.,[27] yielding one dye molecule bound at random for approximately every 300 monomers along the PS chain, as confirmed via absorption spectroscopy. The solvent, Aroclor 1248 (A1248), lot KM 502, is a mixture of chlorinated biphenyl congeners (Monsanto Co.), which was filtered (0.2 μm) prior to use. All solutions were prepared gravimetrically by the direct addition of A1248 to PS. Concentrations were calculated by assuming additivity of volumes and densities of 1.06 and 1.45 g/mL for PS and A1248, respectively. To promote dissolution, the solutions were gently stirred and heated (<50 °C).

Oscillatory Flow Birefringence Measurements. The oscillatory flow birefringence (OFB) apparatus, measurement protocol, and data collection and evaluation have been discussed in detail elsewhere.[2,13] The apparatus is shown schematically in Figure 1. The laser beam (Melles Griot) travels through a Glan-Thompson linear polarizer followed by a quarter-wave plate to generate a circularly polarized beam, which impinges on the sample cell. The emerging beam is divided into the horizontally and vertically polarized components by a Rochon beam-splitting prism (Karl Lambrecht), and the intensities of the two components are monitored by using photodiode detectors (Hammamatsu). The sample is confined to a thin layer between a fixed titanium block and a black glass moving surface. The oscillatory shear is generated by a thin fluid layer transducer (TFL) based on the Miller–Schrag design.[2] Two modifications have been made[13] in the OFB apparatus relative to previous designs: (i) a 5-mW HeNe laser and photodiode detectors have been substituted

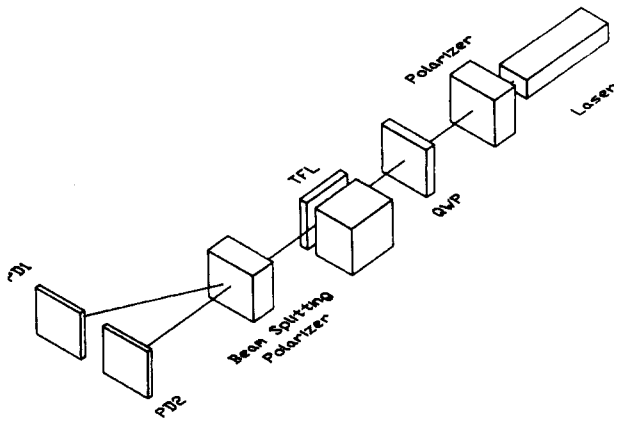

Figure 1. Schematic illustration of the oscillatory flow birefringence apparatus, as described in the text.

for the mercury arc lamp and photomultiplier tube, respectively, and (ii) a double-beam optical configuration has been adopted via the Rochon prism analyzer and two photodiodes, one for each polarization component. The higher photon flux of the laser source relative to the lamp results in an increase in the signal-to-noise ratio. In the double-beam configuration, both the horizontal and vertical components of the transmitted light are monitored simultaneously, thus reducing the effect of source intensity fluctuations. Furthermore, in this configuration the shuttering correction procedure becomes more accurate. (Although the plane oscillates axially, there is inevitably some undesirable lateral component of motion which results in shuttering of the incident beam at the TFL driving frequency. To correct for this shuttering, both horizontal and vertical polarization components of the beam must be monitored.)

The data acquisition and processing system, which has been discussed in great detail previously,[19,28,29] has been tailored for a MassComp (MC-500) computer. The number of data points acquired per (reconstructed) signal cycle at each frequency was at least 1013 and did not exceed 10 000. The number of signal averages varied with the driving frequency and was typically $\simeq 4$ for an 0.1-Hz signal and 256 for a 1-kHz signal. The solution temperatures were maintained to within ± 0.01 °C for the duration of each OFB measurement and were monitored by a thermistor calibrated to ± 0.003 °C relative to a platinum resistance thermometer, with a calibration traceable to NIST. All measurements presented here were obtained with a gap width of 0.3855 mm and an optical wavelength of 632.8 nm.

NMR Measurements. Pulsed-field-gradient spin-echo NMR permits the determination of molecular self-diffusion by applying calibrated, precisely timed magnetic field gradients to the sample. Diffusion coefficients, D, are extracted from measurements of the spin-echo attenuation in response to the applied gradient pulses. The technique has been described elsewhere, as have the calibration procedures, data collection, and data analysis.[30] Proton NMR was detected in the pulsed solid NMR spectrometer, which operated at 33 MHz. These experiments were performed on resonance with digital data collection and screening preceding signal averaging. After application to the sample of a 90° rf pulse (with respect to the applied steady field) and subsequent delay of typically 10 ms during which the gradient is introduced, a second rf pulse is applied following the principal echo two-pulse sequence (90°–180°–echo). This was occasionally supplemented by the three-pulse stimulated echo sequence. The magnetic field gradient pulses were 340 G/cm for up to 16 ms. To stabilize and narrow the echo, a 0.8 G/cm steady gradient was also applied to the sample. For the duration of a particular gradient, results from 10 to 20 echo attenuation measurements were averaged. Values of D were extracted from measurements using varied pulse lengths, with between 5 and 30 points collected at constant gradient pulse magnitude. As a consequence of the short polymer nuclear spin–spin relaxation time, T_2, relative to that of the solvent at lower temperatures, polymer diffusion measurements were performed at 63.5 °C; at this elevated temperature, where all relaxation times exceed the diffusion time, the relative T_2 values are less important. The calibration and

stability of the temperature were better than 0.2 °C. Even for the $M = 3.2 \times 10^4$ PS, the fraction of the spin echo attributable to the polymer was substantially less than the fraction of polymer in the solution, as a consequence of a much shorter T_2 of the long polymer molecules as compared with that of the solvent. Thus, the uncertainties in the D values at higher M and/or lower concentration become particularly large. Reported diffusion coefficients represent averages of two to three independent measurements. The data can be scaled to 25.0 °C via the temperature dependence of the solvent viscosity to compare with the other measured properties.

Forced Rayleigh Scattering Measurements. The details of the forced Rayleigh scattering (FRS) apparatus and measurement technique have been described elsewhere.[31] Briefly, the experiment is performed as follows: an intense Ar^+ laser beam ($\lambda = 457.9$ nm) is divided and recombined to generate an optical interference pattern in the sample. The dye (covalently bound to the polymer) photoisomerizes where the recombined light experiences constructive interference. As the two dye isomers possess different optical properties, an attenuated HeNe laser can then be used to monitor the decay of the diffracted intensity as the optical grating erodes in the sample by interdiffusion. Each decay curve comprises 1000 discrete points collected with 12-bit resolution at equal time intervals. Decay curves were obtained for five or more grating spacings for each solution. To extract the diffusion coefficients, these curves were fit to the form

$$V(t) = \{A \exp(-t/\tau) + B\}^2 + C^2 \quad (1)$$

where $V(t)$ is the time-dependent photomultiplier response; τ is the decay time; and A, B, and C are adjustable parameters corresponding to the diffracted, coherent background, and incoherent background amplitudes, respectively. The diffusion coefficients were determined as the average of two different values, obtained by linear regression from the slopes of (i) decay rate versus inverse grating spacing squared and (ii) decay time versus grating spacing squared. The values determined by the two methods were in agreement to better than 10%. The temperature was maintained at 25.00 ± 0.02 °C, again by use of thermistor with a calibration traceable to NIST. The measurements were performed on A1248 solutions containing a blend of labeled and unlabeled PS (from the same PS lot) in the approximate ratio of 1:4 for the 9.0×10^4 PS and 1:5 for the two lower molecular weight samples, to minimize possible interaction between the dye moieties.

Results

This section is divided into two main parts, one describing the oscillatory flow birefringence data and the other the diffusion results. In the former, the quantities of interest are first defined. Then a discussion of the extraction of polymer dynamics information from solution data is provided, focusing primarily on the correct subtraction of the solvent contribution to the measured solution response. The finite concentration results are then presented, followed by those obtained via extrapolation to infinite dilution. In the second part, the NMR and FRS diffusion data are described.

OFB Data. Definitions. The OFB data are assessed in terms of the complex mechanooptic coefficient, S^*, defined as the ratio of the sinusoidally time varying birefringence (Δn^*) to the sinusoidally time varying shear rate (γ^*). This dynamic shear birefringence can be expressed in phasor notation as

$$S^* \equiv \Delta n^*/\dot{\gamma}^* = S' + iS'' = S_m \exp(i\theta) \quad (2)$$

where S' is the (viscous) in-phase component of the birefringence, S'' is the (elastic) out-of-phase component, S_m is the magnitude, and θ is the phase angle between the birefringence and the shear rate. Rheological properties can also be derived from these optical measurements via the stress-optical relation (SOR).[32] The SOR rests on the assumptions that the refractive index tensor and the stress tensor have (i) identical principal axes, resulting in identical stress orientation and extinction angles, and (ii) proportional differences in principal values. According to the SOR, $C\eta_P^* = S_P^*$, where C is the stress-optical coefficient, η_P^* is the dynamic viscosity, and S_P^* and η_P^* refer to the polymer contributions to the respective dynamic properties. For homopolymer solutions and melts, abundant evidence exists that supports the validity of the SOR, at least for low to moderate frequencies.[8-12,32]

Solvent Contribution to Solution Dynamics. In order to extract the polymer contribution to the solution dynamics, the solvent contribution must first be established. Conventionally, this solvent contribution is taken as $\phi_s S_s$, where S_s is the neat solvent birefringence at a given temperature and ϕ_s is the volume fraction of solvent in the solution. Thus, the polymer contribution to the measured response is determined at each frequency as[2,4-6]

$$S_P^* = S_{soln}^* - \phi_s S_s \quad (3)$$

The solvent is further assumed to act as a viscous continuum and therefore contributes only to S'_{soln} in the frequency range employed here. However, extensive results presented by J. L. Schrag and co-workers demonstrate that eq 3 does not account for the solvent contribution correctly.[7-12,14,16,19,22,23] Similarly, η_s does not account for the solvent contribution to η^*. At high effective frequencies as measured by either OFB or VE techniques, the loss components approach frequency-independent plateaus, designated S'_∞ and η'_∞, respectively.[33] Stokich, Schrag, and others have suggested that it is these quantities which represent the relevant solvent contributions.[11,16] Empirically, the ratio S'_∞/S_s (and η'_∞/η_s) can be greater or less than unity; it is also an approximately exponential function of concentration.[1,3,7-13,19,22] Physically, these observations have been interpreted as reflecting a polymer-induced modification to the properties of the solvent. Recent measurements of the effect of added polymer on the rotational and translational mobility of the solvent have provided direct evidence for this interpretation, at least for Aroclor solutions of polystyrene, polybutadiene, and polyisoprene.[16,30,34] When the solvent contributions are accounted for in this manner, the polymer OFB and VE properties (i) are describable by the bead–spring model over the entire accessible frequency range, (ii) adhere to the SOR, and (iii) are thermorheologically simple (i.e., obey time–temperature superposition). If the "traditional" solvent corrections are used, the resulting polymer properties do not satisfy these three criteria (although the breakdown in any particular criterion may only be observed at relatively high frequencies). Thus, for the purposes of the results to be presented here, S'_∞ is assumed to provide the best estimate of the solvent contribution to S^*_{soln}, and the polymer contribution is extracted accordingly.

The extraction of S'_∞ itself is not a trivial matter, particularly as the high-frequency plateau is only approached at the lowest temperature examined (−1.42 °C) and at the highest effective frequencies measured. Stokich[11] and Landry[8] have described in detail extrapolation methods to obtain S'_∞ from $S'_{soln}(\omega)$ at low temperatures [where ω ($=2\pi f$) is the drive frequency], as well as the subsequent calculation of S'_∞ for higher temperatures. Cast in terms of the BSM parameters

$$S'_{soln}(\omega) = \kappa \sum_{k=1}^{N} \left\{ \frac{\tau_k}{1 + \omega^2 \tau_k^2} \right\} + \begin{matrix}\text{effective solvent} \\ \text{contribution}\end{matrix} \quad (4)$$

where κ is a model-dependent constant, given a particular

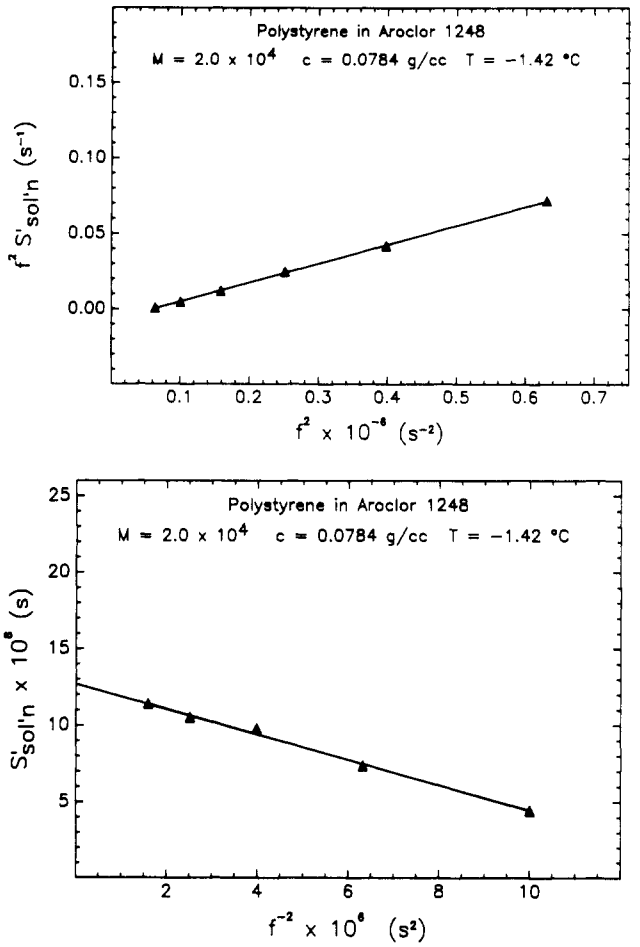

Figure 2. Determination of S'_∞ for a solution of PS (M = 2.0 × 10^4, c = 0.0784 g/mL) in A1248 at −1.42 °C: (a) from the slope of $f^2S'_{soln}$ versus f^2, and (b) from the intercept of S'_{soln} versus f^{-2}.

polymer/solvent system. Equating S'_∞ with the effective solvent contribution, the summation in eq 4 can be approximated for $\omega\tau_N \gg 1$ as

$$S'_{soln}(\omega) \approx S'_\infty + \frac{\kappa}{\omega^2}\sum_{k=1}^{N}\left\{\frac{1}{\tau_k}\right\} = S'_\infty + (\kappa'/\omega^2) \qquad (5)$$

where κ' is a collection of constants. When the data are plotted by following the two different formats $f^2S'_{soln}$ versus f^2 and S'_{soln} versus $1/f^2$, S'_∞ can be extracted as the slope and intercept from the two plots, respectively. The frequency-dependent components of S'_{soln} are emphasized to different extents by the two plotting schemes, and thus averaging the two results improves the accuracy of the determination. An example is shown in Figure 2, parts a and b, for M = 2.0 × 10^4 and c = 0.0784 g/mL. Note that this method of S'_∞ extrapolation does not assume the validity of the BSM per se, but rather that the polymer contribution is expressible as a discrete sum of contributions from various relaxation processes. Values of S'_∞ for the three higher temperature data sets (25.00, 15.88, and 2.81 °C) may then be calculated from S'_∞ (T_{ref} = −1.42 °C) and the relative time–temperature superposition shift factors, a_T, by

$$S'_{\infty,T} = \left(\frac{\rho_T}{\rho_{T_{ref}}}\right)(a_T)(S'_\infty - \phi_s S_s)_{T_{ref}} + \phi_s S_{s,T} \qquad (6)$$

where ρ_T is the density at temperature T.

In Figure 3, values of S'_∞ for T = −1.42 °C are displayed semilogarithmically as a function of c, for PS/A1248. Included in the plot are data for the four M examined here, in addition to data for six other M reported in the literature.[8] Within the experimental uncertainty, S'_∞ is independent of M for PS chains in A1248 when $M \gtrsim 9 \times 10^3$, in agreement with the M dependence exhibited by η'_∞. The values of S'_∞ for the M = 2 × 10^3 sample lie significantly below those for the higher M samples, while for M = 5.5 × 10^3, the values lie slightly below those for higher M. A dashed line representing the traditional solvent correction, $\phi_s S_s$, is also shown in the figure. Clearly, the disparity between $\phi_s S_s$ and S'_∞ increases with increasing concentration, reaching a full order of magnitude by $c \approx$ 0.20 g/mL for $M \geq 9 \times 10^3$.

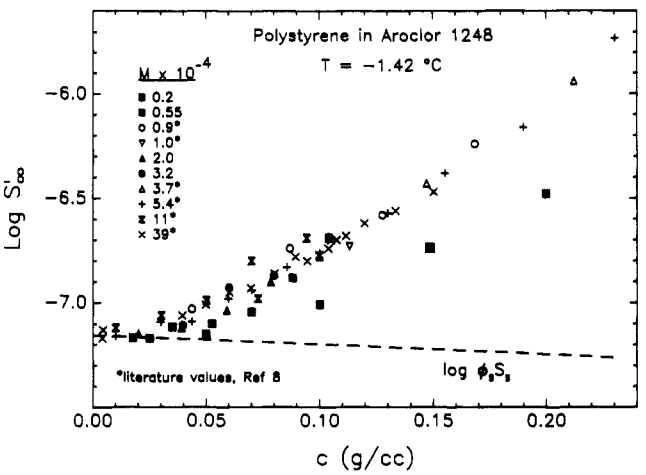

Figure 3. Values of S'_∞ for PS in A1248 at −1.42 °C as a function of concentration, for the indicated molecular weights.

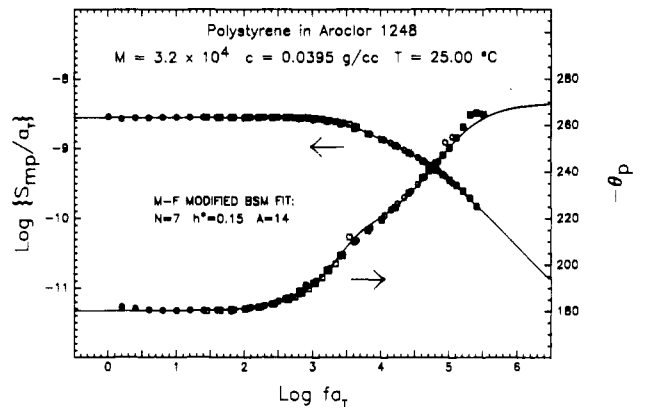

Figure 4. OFB properties for a solution of PS (M = 3.2 × 10^4, c = 0.0395 g/mL) in A1248, compared with the predictions of the MF theory.

Polymer Contribution to Solution Dynamics: Finite Concentration Data. For the remainder of the paper, the effective solvent contribution is taken to be S'_∞, and the polymer contribution to S^*_{soln} extracted accordingly. Values of S'_∞ were obtained at −1.42 °C by the procedure detailed in the previous section, whereas those at the other three measurement temperatures (2.81, 15.88, and 25.00 °C) were obtained via eq 6. For a given M and c, the data at each of the four temperatures were combined via time–temperature superposition to provide one master curve, with T_{ref} = 25.00 °C. An example is shown in Figure 4, for M = 3.2 × 10^4 and c = 0.0395 g/mL; the data are plotted as log (S_{mP}/a_T) and θ_P versus log fa_T. The shift factors were determined empirically, relying primarily on the low-frequency limiting value of S_{mP}, $(S_{mo})_P$, which was accessible for almost all the concentrations and temperatures employed, as a consequence of the low values of M. There exists a substantial body of OFB and VE data for predominantly higher molecular weight PS in A1248 than those considered here, and for

which the values of a_T have been tabulated;[11] a_T is found to be independent of M, but an increasing function of c, for these measurement temperatures. The values obtained here are within experimental uncertainty equal to those reported previously. The theoretical curves in Figure 4 will be discussed subsequently.

Of the four samples studied, each at five different c, only the data for the lowest c (0.0250 g/mL) of the lowest M (2×10^3) did not superpose well. The observed birefringence signal decreases with M and c, rendering the data for this solution the least certain of all those measured. Although A1248 is not strongly birefringent, its contribution to the measured response exceeded that for the polymer at all frequencies evaluated for three solutions examined: c = 0.0250 and 0.0499 g/mL for $M = 2 \times 10^3$, and c = 0.0175 g/mL for $M = 5.5 \times 10^3$ PS. The sign of the solvent birefringence is positive, whereas that for the polymer is negative. Thus, when the magnitude of the solvent contribution approaches that of the polymer, the net solution birefringence can approach zero, making the extraction of the polymer contribution particularly precarious. For the three dilute solutions of low M mentioned above, S'_{soln} was positive for all frequencies measured.

Examination of eq 6 reveals that to determine values of S'_∞ at the higher temperatures, the values of a_T must be known. However, the values of a_T obtained will in principle depend on the solvent correction employed, suggesting the possibility of an iterative procedure. In fact, for sufficiently high M samples, the values of $(S_{mo})_P$ obtained do not vary significantly with the magnitude of the solvent correction; thus the a_T values are not sensitive either, and consequently such iteration is not necessary. On the other hand, for the lowest M sample examined here, 2×10^3, and the two lowest c, it was necessary to recalculate a_T after first estimating the values of S'_∞ via eq 6, and then to repeat the calculation of the polymer contribution.

Polymer Contribution to Solution Dynamics: Infinite Dilution Properties. To compare directly with the BSM predictions the OFB data must first be extrapolated to infinite dilution, as the original model incorporates no polymer/polymer interaction terms. A variety of extrapolation schemes have been reported and discussed in the literature, both for OFB and VE properties;[1,4,6,8,10,13,14] however, for data of sufficient precision and adequately low c, the resulting intrinsic values are sensibly independent of the extrapolation method. For the majority of the data considered here, the extrapolations were performed as log $(-S'_P/c)$ and log (S''_P/c) versus c; the minus sign is simply a consequence of the negative stress-optical coefficient for PS. The extrapolations uniformly display the high precision demonstrated previously for OFB measurements on PS in A1248 and are therefore not shown here.[1,4,6,8,10,13,14] For the two lower c with $M = 2 \times 10^3$, the data were excluded from the extrapolations due to the larger uncertainty. After the intrinsic quantities $[S']_P$ and $[S'']_P$ were determined in this fashion, $[S_m]_P$ and $[\theta]_P$ were calculated and then reduced to master curves via time–temperature superposition. Figures 5–7 present the resulting infinite dilution master curves for the three highest M, along with theoretical curves whose significance will be discussed subsequently. The intrinsic properties for the shortest chain, $M = 2.0 \times 10^3$, were not sufficiently precise to justify extensive analysis at this point.

Diffusion Data. NMR. Among the strengths of NMR as a technique for measuring diffusion coefficients are the absence of a need for chemical labeling and the absence of any imposed concentration gradients. On the other hand, there are weaknesses that are particularly relevant in the PS/A1248 case. First, the high solvent viscosity renders D too small to be measured for higher M. Second, the contribution from the solvent limits the precision for low polymer concentrations ($\lesssim$0.05 g/mL). Third, extrapolation to infinite dilution requires measurements in dilute solutions, which can only be achieved for low M under the previous concentration restriction. Nevertheless, it was possible to measure D and extrapolate to infinite dilution for four M, ranging from 2×10^3 to 3.2×10^4, at 63.5 °C. The data are presented in Figure 8, as log D versus c; the values of D_0, the intercepts obtained by linear regression, are listed in Table II. The NMR values of D_0 have been scaled to 25.0 °C by the ratio of the quantity (T/η_s), determined from the temperature dependence of η_s reported by Merchak.[10] This scaling assumes that there is no change in the hydrodynamic radius of the polymer

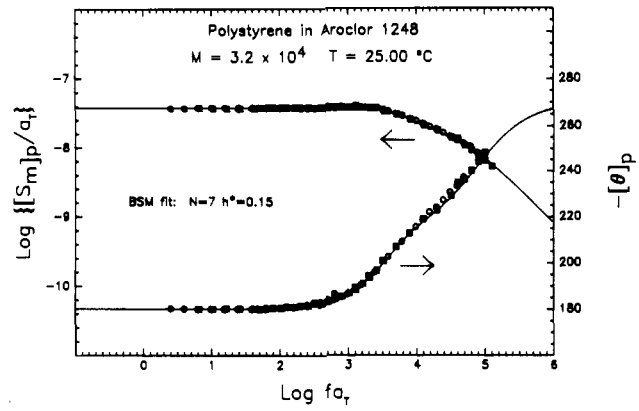

Figure 5. Infinite dilution OFB properties for PS ($M = 3.2 \times 10^4$) in A1248, compared with the predictions of the BSM.

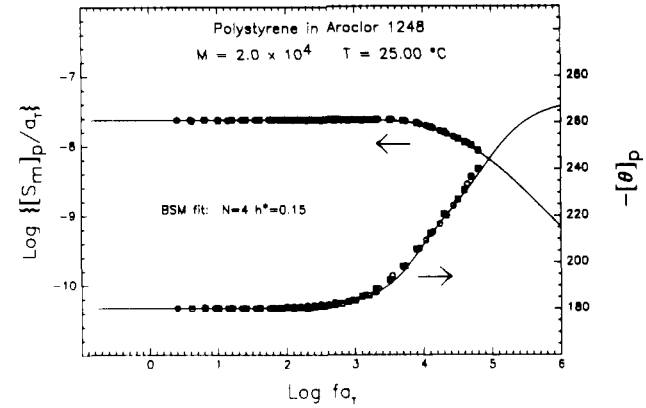

Figure 6. Infinite dilution OFB properties for PS ($M = 2.0 \times 10^4$) in A1248, compared with the predictions of the BSM.

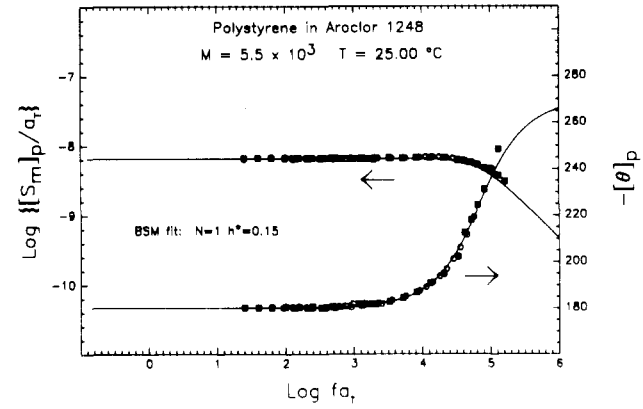

Figure 7. Infinite dilution OFB properties for PS ($M = 5.5 \times 10^3$) in A1248, compared with the predictions of the BSM.

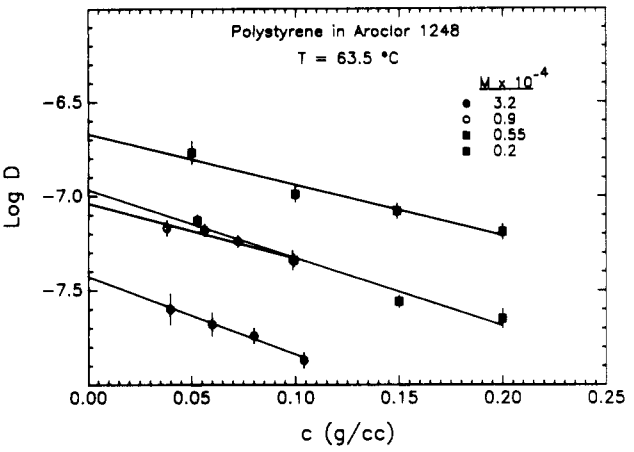

Figure 8. PS diffusivity versus concentration for PS in A1248 at 63.5 °C, for the indicated molecular weights, determined by NMR.

Table II
Diffusion Data[a]

$M \times 10^{-4}$	D_0 (25.0 °C), cm^2/s	measurement technique	$M \times 10^{-4}$	D_0 (25.0 °C), cm^2/s	measurement technique
0.2	1.4×10^{-8}	NMR	3.2	2.3×10^{-9}	NMR
0.55	6.8×10^{-9}	NMR	3.2	2.3×10^{-9}	FRS
0.9	5.8×10^{-9}	NMR	9.0	1.3×10^{-9}	FRS
0.9	4.6×10^{-9}	FRS			

[a] 25.0 °C NMR data have been scaled from 63.5 °C data.

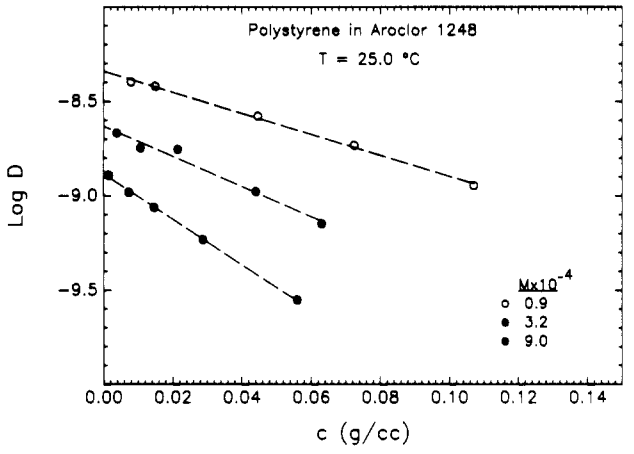

Figure 9. PS diffusivity versus concentration for PS in A1248 at 25.0 °C, for the indicated molecular weights, determined by FRS.

with T. Given the relatively low M employed and the fact that A1248 is a moderately good solvent for PS, this assumption is reasonable; in light of the uncertainty in the measured D values, it is even less of a concern.

FRS. In contrast to NMR, FRS is almost ideally suited for determining D_0 in the PS/A1248 system. Polymer concentrations as low as 0.1% give a large signal, at least with this particular dye and labeling level, and very small diffusion coefficients are accessible. The major experimental difficulty is the introduction of the dye label, which must be achieved without degradation of the narrow molecular weight distribution. The values of D obtained at 25.00 °C for three M are plotted logarithmically as a function of c in Figure 9. Values of D_0 were obtained by linear regression and are listed in Table II. Note that two of the FRS samples ($M = 9.0 \times 10^3$ and 3.2×10^4) were also examined by NMR. For the higher M, the two techniques agree very well, while for the lower M sample the NMR value lies 25% above the FRS datum.

Discussion

This section is organized in the following manner. First, the bead–spring model (BSM) is briefly reviewed, particularly in relation to the predictions for the OFB properties. Second, the frequency dependence of the infinite dilution OFB results is evaluated in terms of the BSM parameters, N and h^*. Third, the finite concentration OFB data are compared with the Muthukumar–Freed extension of the BSM.[35] Fourth, the longest relaxation time, τ_1, is extracted from both the finite concentration data and the infinite dilution results. Following this analysis of the OFB data, the polymer diffusivities are examined in the BSM framework, via the Kirkwood–Riseman expression.[36] The OFB and diffusion results are then combined with R_g and $[\eta]$ values from the literature to provide an initial assessment of the self-consistency of the BSM.

Bead–Spring Model (BSM). The BSM, a statistical mechanical theory pioneered by Rouse and Zimm,[24] was designed to describe the infinite dilution viscoelastic properties of flexible, long-chain macromolecules. In the model, the actual polymer chain is replaced by $N + 1$ beads connected by N Hookean springs. The model chain is freely jointed and each bead–spring unit represents a Gaussian subchain of the actual macromolecule; i.e., a subchain represents a sufficient number of monomers such that the subchain end-to-end vector obeys Gaussian statistics. Each spring has a root-mean-square length, b, and a friction coefficient, ζ, is associated with each bead. The model chain is immersed in a solvent taken to be a Newtonian continuum with viscosity η_s.

The three independent parameters of the BSM are thus N, b, and ζ; either of the latter two parameters may be replaced by h^*, the so-called hydrodynamic interaction parameter, defined as[37]

$$h^* = \zeta/(12\pi^3)^{1/2} b\eta_s \tag{7}$$

The BSM can be used to make explicit predictions for all of the measured properties presented in this report. In terms of the BSM parameters, the dynamic shear birefringence defined in eq 2 can be written as

$$S^* = \pm q'\left(\frac{N_a c}{M}\right) b^2 \sum_{k=1}^{N} \left\{\frac{\tau_k}{1 + i\omega\tau_k}\right\} + \text{solvent contribution} \tag{8}$$

where N_a is Avogadro's number, $i = (-1)^{1/2}$, and q' is an optical factor given by

$$q' = \frac{4\pi}{45}\left(\frac{n_s^2 + 2}{n_s}\right)^2 \left(\frac{\alpha_1 - \alpha_2}{b^2}\right) \tag{9}$$

where n_s is the solvent refractive index and $(\alpha_1 - \alpha_2)$ is the polarizability anisotropy of a subchain. As discussed under Results, the solvent contribution is represented as S'_∞ in this work.

Before discussing the comparison of the predictions of eq 8 with the data in Figures 5–7, a few general features of the BSM are first mentioned with regard to its application to the interpretation of OFB data. The primary strengths of the BSM are that it is (i) a physically plausible model for the dynamics of isolated flexible chains; (ii) exactly solvable (numerically) for arbitrary values of the parameters; and (iii) extendable to more complicated systems, for example, branched chains,[17,20] cyclic chains,[20] and block copolymers.[21–23] The limitations of the BSM are also substantial; among the most prominent are (i) the failure to account explicitly for excluded volume effects,

(ii) the failure to predict shear-thinning at higher shear rates, and (iii) a rather crude representation of the local dynamics of the chain. For the purposes of the ensuing analysis, however, only the last of the three limitations is potentially serious. In terms of (i), for example, it has been established experimentally that the static structure factor for PS in A1248 is well-represented by the Debye function, at least for $M \leq 10^5$,[25] and that therefore the monomer distribution function is at least approximately Gaussian. Furthermore, allowing h^* to vary has been shown to be quite successful in describing changes in the relaxation spectrum due to changes in solvent quality.[1,5,6,14,20] A variety of approximate schemes to account for excluded volume in the BSM have been developed; however, all require specification of at least one more parameter.[20,38] In this report we are focusing on assessing the self-consistency of the BSM in its simplest form. Relative to (ii), we are concerned with the regime of linear viscoelasticity, and therefore nonlinear effects are not of concern.

Infinite Dilution OFB Properties. The infinite dilution intrinsic quantities, $[S_m]_P$ and $[\theta]_P$, are plotted as functions of reduced frequency in Figures 5–7, for $M = 3.2 \times 10^4$, 2.0×10^4, and 5.5×10^3, respectively. The smooth curves represent predictions of the BSM, with parameter values (N and h^*) as indicated. For all three samples, time–temperature superposition appears to work very well. For the two highest M samples, the theoretical curves describe the results extremely well over the entire experimental frequency range; the agreement for the $M = 5.5 \times 10^3$ sample is somewhat less satisfactory, but still quite reasonable. For the $M = 2.0 \times 10^3$ sample (data not shown), the superposition is less than satisfactory, as noted under Results, and the BSM fit to the infinite dilution properties is also poor. This reflects primarily the uncertainty in extracting the small polymer contributions from the measured solution properties, compounded with the error inherent in an extrapolation procedure. Therefore, the only information that could be extracted reliably from these data are the values of the longest relaxation time, τ_1, as a function of c and at infinite dilution, as will be discussed subsequently.

Although only two parameters (N and h^*) are specified in Figures 5–7, in fact four parameter values are necessary to compare the BSM calculations with the data quantitatively. The other two are $[S_{mo}]_P$ (or equivalently, q' in eq 8) and b (or ζ). These establish the vertical position of the S_{mP} curve and the absolute frequency scale for the horizontal axis, respectively. Values of the former have been discussed elsewhere,[11,26] whereas values of the latter will be addressed in the discussion of τ_1. The values of N and h^* determine the eigenvalues of the Zimm **H·A** matrix (or Lodge–Wu **B** matrix[39]), and thus the breadth and spacing of the relaxation spectrum, $\{\tau_k\}_{k=1,2,...,N}$. Specifically, the breadth of the spectrum is controlled primarily by N, while the value of h^* influences the relative spacings among the relaxation times. In the free-draining or Rouse limit, $h^* = 0$, and the relaxation times scale approximately with k^2 (particularly for large N and small k), as is well-known. The principal effect of increasing h^*, up to the non-free-draining or Zimm limit of $h^* \approx 0.25$, is to decrease the spacing between successive relaxation times. In general, there is little interaction between N and h^* when BSM calculations are compared with the OFB data; in other words, the effect on the predicted OFB properties of changing N cannot be duplicated by changing h^*, and vice versa. Therefore, "best-fit" values for both parameters may be uniquely determined visually. For all values of M considered here, and for values of M up to 1.8×10^6 presented elsewhere,[4,14] the appropriate value of N can be determined to within ±1 or 2. For higher M samples, h^* may be determined to within ±0.01 to 0.02. For the low M samples considered here, the N values are so small (<10) that the value of h^* has relatively little effect on the theoretical curves. A value of $h^* = 0.15$ has been selected, based on extensive prior measurements for $5 \times 10^4 < M < 1.8 \times 10^6$; a value of $h^* = 0.175$, which has been employed in some cases for PS/A1248, would also be satisfactory to describe these data. Values for N of 7, 4, and 1 have been used to describe the results for $M = 3.2 \times 10^4$, 2.0×10^4, and 5.5×10^3, respectively, corresponding to an apparent subchain molecular weight, M_s, of approximately 5×10^3. This value of M_s is also in good agreement with those inferred from higher M samples, particularly when the inevitable uncertainty ($\simeq 10\%$) in the M values themselves is recalled; for example, a value of 4.3×10^3 has recently been proposed.[14] The exact value of M_s is also dependent on whether a polydispersity correction is included in the BSM calculations.[14] Additionally, in a previous publication the infinite dilution OFB properties determined for a sample with $M = 1.0 \times 10^4$ were examined, and values of $N = 2$ and $h^* = 0.15$ described the data well.[4]

The most surprising feature of the results in Figures 5–7, and indeed for the finite concentration OFB results as well, is the apparent distinct "end" to the relaxation spectrum. In other words, $[\theta]_P$ or θ_P can only approach $-270°$ for $\omega\tau_N > 1$, i.e., at frequencies higher than the inverse of a "shortest" relaxation time. (A substantial gap in the relaxation spectrum could also have the same effect.) The data approach $-270°$ more closely for finite concentrations, and for higher M samples,[2,4-8,12-14] than do the results in Figures 5–7, due to reduced signal-to-noise ratios, but the results as a whole are completely consistent on this point. It is for this reason that a specific, finite value of N is required to describe the frequency dependence of the OFB and VE properties for a given M. The resulting apparent value of M_s corresponds to a subchain of approximately 50 monomer units, which is surprisingly large. Taken literally, this suggests that no conformational relaxations take place on a shorter length scale. However, the characteristic ratio for PS implies a persistence length closer to 10 monomer units, clearly indicating that motions on a shorter length scale must occur. Thus, the appropriate question is why these motions are not evident in the conformational dynamics experiments. As yet, no clear answer has emerged.

One issue to consider is the dynamics of the solvent in the neighborhood of the chain. As pointed out previously, it is clear that the reorientational mobility of the A1248 molecules is significantly retarded by the presence of the PS chains.[34] The A1248 molecular dimensions are within a factor of 2–3 of R_g for a 50 monomer PS chain, and furthermore, A1248 as a glass-forming liquid ($T_g \approx -44$ °C[34]) may well exhibit significant intermolecular orientational correlation. Thus, it is conceivable that dynamic rigidity in the solvent may inhibit relative polymer/solvent motion; this possibility is clearly quite speculative. It is clear, however, that the modified solvent contribution and concomitant subtraction scheme are not the primary cause of the large apparent value of M_s; the fact that S'_∞ and η'_∞ reflect predominantly properties of the solvent has been well-established.[7-12,14,16,19,22,23,34]

OFB Finite Concentration Results. The range of applicability of the BSM has been extended to finite concentrations by Freed and Edwards,[40] Muthukumar and Freed,[35] Freed and Perico,[41] and most recently by Muth-

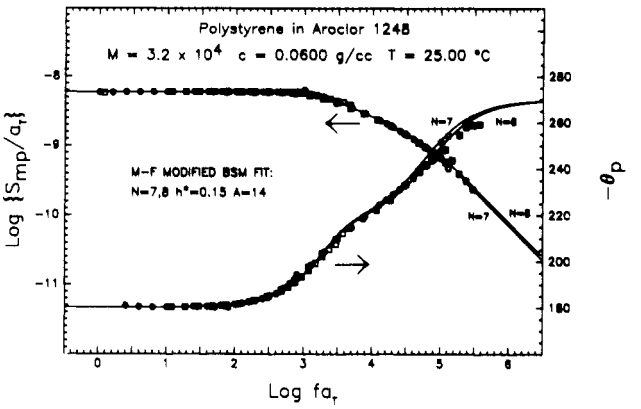

Figure 10. OFB properties for a solution of PS ($M = 3.2 \times 10^4$, $c = 0.0600$ g/mL) in A1248, compared with the predictions of the MF theory.

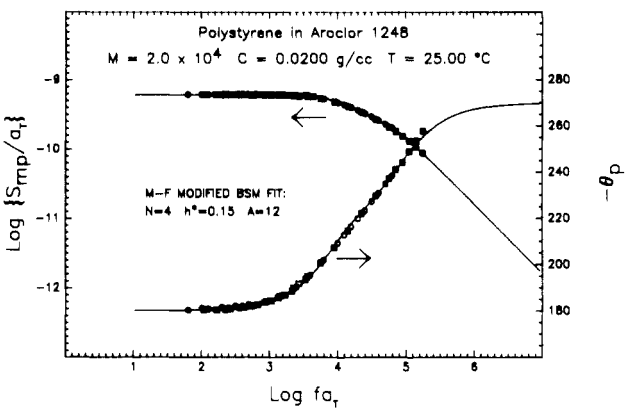

Figure 11. OFB properties for a solution of PS ($M = 2.0 \times 10^4$, $c = 0.0200$ g/mL) in A1248, compared with the predictions of the MF theory.

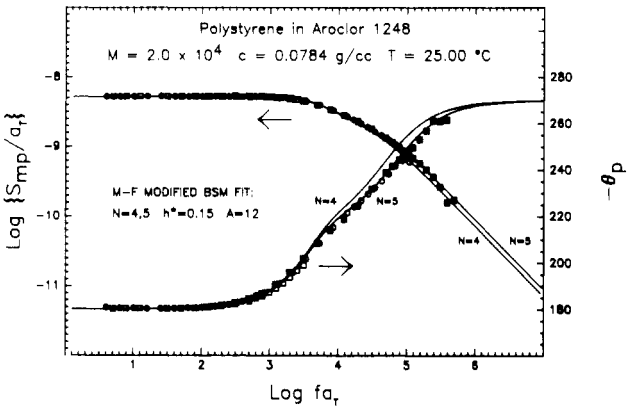

Figure 12. OFB properties for a solution of PS ($M = 2.0 \times 10^4$, $c = 0.0784$ g/mL) in A1248, compared with the predictions of the MF theory.

ukumar.[42] As the Muthukumar and Freed (M–F) modification is adequate to describe the data examined here and is also simpler in form than the others, only the M–F modification is utilized in this report. The initial concentration dependence of the relaxation times in the M–F analysis is given as

$$\tau_k = \tau_k^\circ[1 + cAk^{-\kappa} + ...] \qquad (10)$$

where τ_k° refers to the infinite dilution (BSM) value of the kth relaxation time, A is a molecular weight dependent parameter proportional to the product of $[\eta]$ and the Huggins coefficient, and κ is an exponent analogous to the Mark–Houwink intrinsic viscosity exponent. The values of both A and κ vary with the extent of excluded volume, and therefore with solvent quality as well. Thus, for a Θ system, $\kappa \approx 0.5$, whereas for a good solvent, κ may range from approximately 0.65 to 0.80. As A1248 is considered to be a moderately good solvent for PS, κ has been assigned the value 0.65, following the results of Lodge and Schrag;[5] however, the predictions are relatively insensitive to values of κ, especially for small values of N. From eq 10, it is apparent that in the M–F expression higher modes of motion are progressively less sensitive to c. Physically, this description is quite reasonable, as the higher modes correspond to relaxations on shorter length scales. Such motions require smaller volumes than those involving longer chain segments and, therefore, will be less strongly influenced by the presence of other chains. Previously, the M–F modified BSM predictions have provided excellent descriptions of the experimental results when applied to PS/A1248 solutions with $M = 3.9 \times 10^5$, and for which $c[\eta] \lesssim 1$. The agreement with the data is still reasonable, although not as good, when $1 \lesssim c[\eta] \lesssim 2$. For the solutions examined here, $0.15 \lesssim c[\eta] \lesssim 1.4$.

In Figure 4, the OFB properties for a solution ($c = 0.0395$ g/mL) of the $M = 3.2 \times 10^4$ PS were presented, along with the M–F theoretical curves. The values of N and h^* were retained from the infinite dilution analysis (Figure 5) and the parameter A was chosen as 14 mL/g, based on the $\tau_1(c)$ behavior discussed in the next section. For this solution, $c[\eta] \approx 0.9$, based on $[\eta]$ values from the literature.[26] The agreement between theory and experiment is very good over the entire frequency range. However, when c is increased to 0.0600 g/mL, and $c[\eta] \approx 1.3$, the quality of the fit deteriorates, as shown in Figure 10. In essence, the c dependence of the relaxation times is stronger than linear. Qualitatively, the effect is comparable to increasing the breadth of the relaxation spectrum by increasing N; a curve with $N = 8$ matches the data more closely than one with $N = 7$.

In Figures 11 and 12, data for $M = 2.0 \times 10^4$ at two concentrations ($c = 0.0200$ and 0.0784 g/mL) are shown, along with the corresponding M–F predictions. Here, A is chosen to be 12 mL/g. For the lower c data displayed in Figure 11, where $c[\eta] \approx 0.4$, the agreement is again excellent. For the higher c data displayed in Figure 12, where $c[\eta] \approx 1.3$, the agreement is much less satisfactory. Also shown is the theoretical curve with N incremented by 1, i.e., $N = 5$, which corresponds more closely to the data. Increasing the value of A, however, would not result in closer agreement, at least not without compromising the quality of the fits at lower c.

For $M = 5.5 \times 10^3$, the infinite dilution results were well-described by a BSM curve with $N = 1$, implying that there is only one relaxation time. In this case, the M–F modification has no effect on the shape of the relaxation spectrum; changes in A are reflected only in the c dependence of τ_1. In Figure 13, the data for this sample with $c = 0.0700$ g/mL, $c[\eta] \approx 0.6$, are plotted. The data fall between BSM curves drawn with $N = 1$ and $N = 2$, again suggesting an increase in the breadth of the relaxation spectrum with increasing concentration. This is, in fact, not too surprising, given these small values of N. The two general conclusions that may be drawn from the data and predictions in Figures 4 and 10–13 are that (i) the M–F modification to the BSM provides an excellent description of the initial c dependence ($c[\eta] < 1$) of the relaxation spectrum, even for these very low M, but that (ii) with increasing c, the number of "visible" relaxation modes appears to increase.

Longest Relaxation Time. Values for the longest relaxation time, τ_1, for all four M are shown in Figure 14,

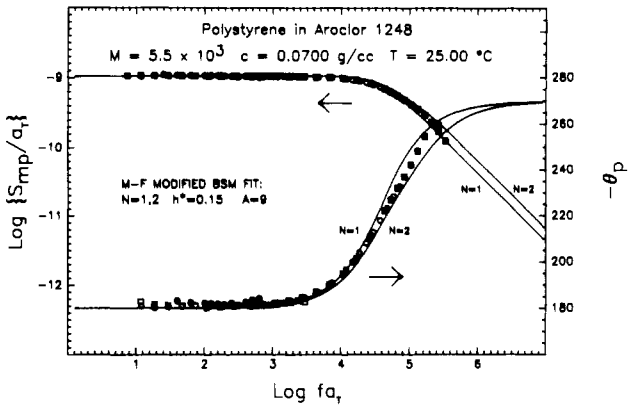

Figure 13. OFB properties for a solution of PS ($M = 5.5 \times 10^3$, $c = 0.0700$ g/mL) in A1248, compared with the predictions of the MF theory.

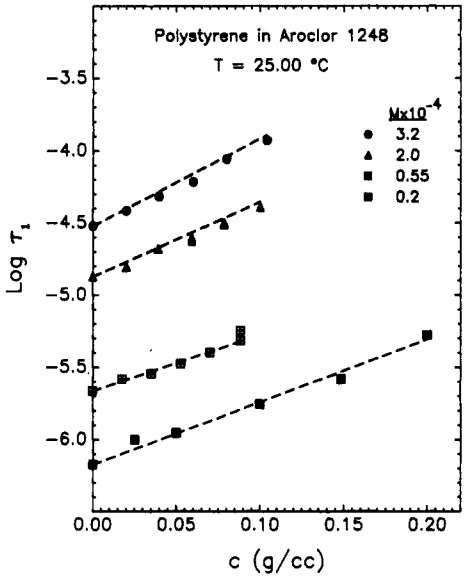

Figure 14. Longest relaxation time versus concentration for PS in A1248 at 25.00 °C, for the indicated molecular weights.

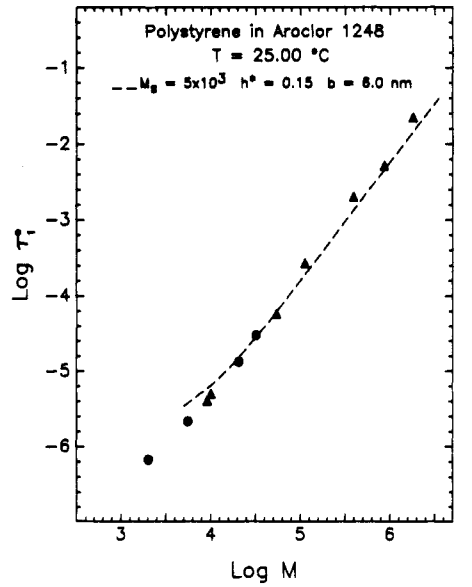

Figure 15. Infinite dilution longest relaxation time[4,5,8,14] versus molecular weight for PS in A1248 at 25.00 °C, compared with the predictions of the BSM.

as a function of c. For the three highest M samples, $\tau_1(c)$ was obtained by comparing the OFB data with M–F theory curves. Although at the higher c the predictions do not match the data over the entire accessible frequency range, values of $\tau_1(c)$ were extracted after the agreement in the low-frequency region was optimized; these values are rather insensitive to small variations in the BSM parameters (N, h^*) chosen. For these three samples, the infinite dilution values of τ_1 in Figure 14 were similarly obtained from the BSM fits in Figures 5–7. For the lowest M sample, the difficulties in extracting the polymer contribution, particularly at low c, rendered the determination of $\tau_1(c)$ uncertain. Therefore, an alternate scheme was employed. Because the data for this sample appeared to be dominated by a single relaxation process, $\tau_1(c)$ can be taken as the inverse of the frequency where the elastic component, S''_P exhibits a maximum. As the solvent contributes only to S'_{soln}, this method circumvents the difficulties described previously. For the three highest c, it was also possible to use BSM curves to extract τ_1; both approaches yielded equivalent results. Furthermore, the alternate method (maximum in S''_P) was applied to the $M = 5.5 \times 10^3$ solutions, and again the values of $\tau_1(c)$ obtained by the two methods were equivalent.

From eq 10, the M–F theory predicts an initially linear c dependence for τ_1. In Figure 14, however, the data (plotted semilogarithmically) are reasonably well described by an exponential dependence, i.e., $\tau_1 = \tau_1^\circ \exp(Ac)$. Similar observations have been reported for a variety of other M.[6,8,12] From Figures 4 and 10–13, the M–F predictions describe the c dependence of the breadth of the relaxation spectrum quantitatively up to $c[\eta] \approx 1$; however, for $\tau_1(c)$ higher order terms omitted from eq 10 apparently become significant even for $c[\eta] < 1$. The straight lines in Figure 14 represent the exponential dependence suggested above, using the corresponding values of A employed in Figures 4 and 10–13. It should be emphasized that this (approximately) exponential dependence is empirical, although it has been rationalized by a scaling argument.[43] At the higher c in Figure 14, as well as in previous studies involving larger values of M and/or $c[\eta]$, deviations from this exponential dependence have been observed.[6,8,12]

The infinite dilution values of the longest relaxation time, τ_1°, are compared directly with BSM predictions in Figure 15. Here, τ_1° is plotted versus M in a double-logarithmic format; also included are values for other M,[4,8,14] obtained in a similar manner. The BSM prediction for τ_1° may be written as

$$\tau_1^\circ = [b^2\zeta/6kT]\lambda_1^{-1}(N,h^*) \qquad (11)$$

where λ_1 is the first (nonzero) eigenvalue of the Zimm **H·A** matrix. Once a value for h^* has been selected, either b or ζ may be adjusted to obtain the best agreement with the data. The slope of the log τ_1° versus log M curve at high M depends on the value of h^*, varying between 1.5 ($h^* = 0.25$) and 2.0 ($h^* = 0$). Following Figures 5–7, M_s is taken as 5×10^3, and h^* as 0.15. By selecting a value of 6.0 nm for b, the theoretical curve displayed in Figure 15 is generated; the curve stops at $M = 5 \times 10^3$, corresponding to $N = 1$. Clearly, the BSM is able to provide a good description of the M dependence of τ_1° over this range, with the same parameters as used to describe the frequency dependence of S_P^*. At this stage, the set of three parameters (N, b, and ζ) is established, and it is interesting to ask whether the M dependence of D_o, R_g, and $[\eta]$ can be similarly well-described with the same parameter values.

Diffusivity. The Kirkwood–Riseman expression[36] for the translational diffusion coefficient of a chain at infinite

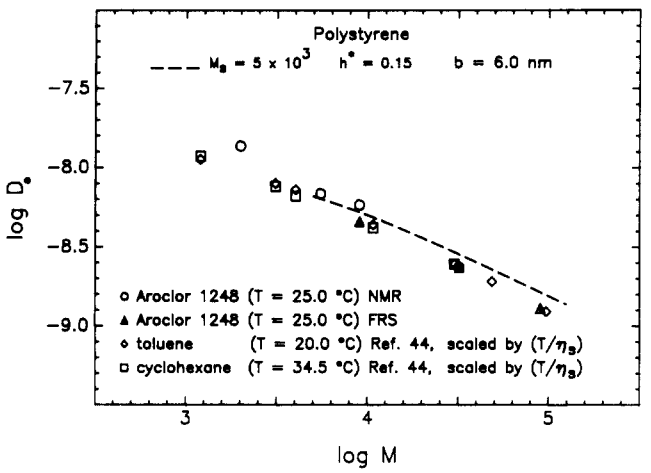

Figure 16. Infinite dilution diffusivity for PS versus molecular weight, compared with the predictions of the BSM.

dilution may be written as[44]

$$D_o = \left(\frac{kT}{\zeta}\right)\left\{\left(\frac{1}{N+1}\right) + \left(\frac{1}{N+1}\right)^2\left(\frac{\zeta}{6\pi\eta_s}\right)\sum_{i}^{N+1}\sum_{j\neq i}^{N+1}\left\langle\frac{1}{r_{ij}}\right\rangle_{eq}\right\} \quad (12)$$

where r_{ij} is the distance between the ith and jth beads, and the average is taken over the equilibrium distribution function (in the preaveraging approximation). Note that the summation is over the number of beads in the chain, and thus $N + 1$ is the correct upper limit. The first term on the right-hand side of eq 12 is the Rouse or free-draining contribution, whereas the second term represents the Zimm or non-free-draining contribution. For a Gaussian chain, the latter becomes $3.77h^*/(N+1)^{0.5}$ in the limit of large N. For the range of N considered here, the summation should be performed explicitly and can be simplified by rewriting eq 12 as[44]

$$D_o = \left(\frac{kT}{\zeta}\right)\left\{\left(\frac{1}{N+1}\right) + \left(\frac{1}{N+1}\right)^2(2^{1.5}h^*)\sum_{j}^{N}\left[\frac{N+1-j}{j^{0.5}}\right]\right\} \quad (13)$$

The experimental values of D_o, listed in Table II, are plotted as a function of M in Figure 16, in a double-logarithmic format. Additionally, several values of D_o for PS in toluene (a good solvent) and cyclohexane (a Θ solvent) are shown for comparison. These data were obtained by Huber et al.[44] via dynamic light scattering and have been scaled by the factor (T/η_s) to make the comparison quantitative. The data presented here are in excellent agreement with those of Huber et al., and furthermore, no substantial effect of solvent quality is apparent over this M range. This provides additional justification for applying the Gaussian chain result (eq 13) to the PS/A1248 data. In the preceding sections, the infinite dilution OFB results (both in terms of τ_1 and $\{\tau_k\}$) were very well described by the BSM with $M_s = 5 \times 10^3$, $h^* = 0.15$, and $b = 6.0$ nm. As the preaveraged Kirkwood–Riseman hydrodynamics are incorporated into the BSM, the diffusion data may be compared with eq 13 and evaluated with these parameter values. The resulting prediction is shown in Figure 16. The agreement between experiment and theory is really quite good, especially given that no parameter values were adjusted. However, the Gaussian chain assumption in eq 13 guarantees that $D_o \sim M^{-0.5}$ at high M, whereas for a moderately good solvent an eventual crossover to $D_o \sim M^{-0.6}$ is expected. Further FRS measurements will be required to investigate this issue.

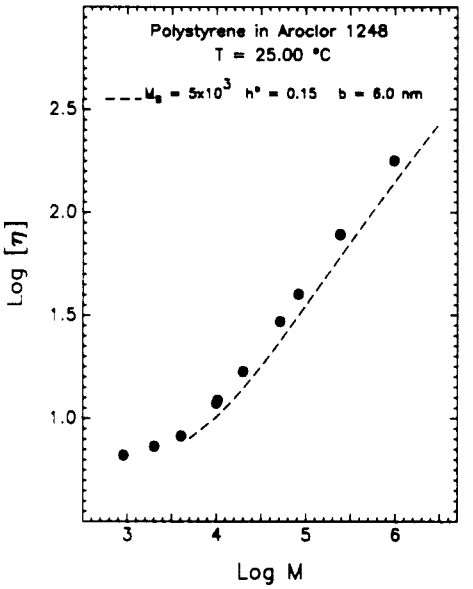

Figure 17. Intrinsic viscosity versus molecular weight[26] for PS in A1248 at 25.00 °C, compared with the predictions of the BSM.

The parameter values listed above correspond to a bead friction coefficient, ζ, of 3.75×10^{-6} g/s. This may be compared to a monomeric friction coefficient of 3.8×10^{-7} g/s, estimated from the diffusivity of azobenzene in the neat solvent at the same temperature.[30] In other words, the solvent diffusivity is $\simeq$1 order of magnitude larger than that for a PS chain with $M = 5 \times 10^3$. It should also be noted that there exist several different ways to describe the diffusion of short chains, for example, those such as the helical wormlike chain of Yamakawa, which take account of the effects of chain stiffness.[45] To explore these in detail is beyond the scope of this article, in which we are trying to compare a broader set of experimental measurements within one theoretical framework. But it is important to emphasize that there is no reason to suppose that eq 13 provides the best possible description of D_o for short chains.

Self-Consistency of the BSM. The OFB and diffusion results presented above indicate that for PS in A1248, the BSM provides a quantitative description of the chain dynamics at infinite dilution, at least for $5 \times 10^3 < M \leq 10^5$. Two other properties, $[\eta]$ and R_g, have previously been examined for this system. In Figure 17, the intrinsic viscosity results as a function of M are reproduced,[26] along with the BSM prediction:

$$[\eta] = \left(\frac{RT}{M\eta_s}\right)\sum_{k}^{N}\tau_k \quad (14)$$

The parameter values $M_s = 5 \times 10^3$, $h^* = 0.15$, and $b = 6.0$ nm were retained from the previous results. The M dependence of $[\eta]$ is very well represented by eq 14 with these parameters (the slope depends rather sensitively on the value of h^*), but the magnitude is slightly underestimated. The agreement could be improved markedly by changing M_s or b, but this is not attempted here. Rather, it should be noted that these values of $[\eta]$ have been determined in the traditional way, namely, as

$$[\eta] = \lim_{c\to 0}\left\{\frac{\eta - \eta_s}{c\eta_s}\right\} \quad (15)$$

where η is the measured solution viscosity. However, as

discussed previously, the solvent contribution is more properly given by η'_∞. At high M, where η'_∞ is independent of M, replacing η_s with η'_∞ in eq 15 would result in values of $[\eta]$ that are approximately 14 mL/g lower. This adjustment would bring the results into closer agreement with the theoretical curve in Figure 17. At low values of M (i.e., $M \leq 2 \times 10^4$), the adjustment is more uncertain, because the values of η'_∞ are comparable to the measured solution viscosities themselves. In short, the BSM may provide a quantitative description of $[\eta]$ as well, once the appropriate solvent contribution is taken into account. In support of this suggested adjustment, it should be noted that the values of the Flory constant, Φ ($=M[\eta]/6^{1.5}R_g^3$), obtained with the "uncorrected" $[\eta]$, lie in the range (3.5–5) $\times 10^{23}$ mol^{-1}, whereas use of the "corrected" $[\eta]$ gives Φ in the range (2–3) $\times 10^{23}$ mol^{-1}.[13] The latter values are in much better agreement with theory, and with experiments on higher molecular weight polymers in a variety of solvents.[46]

The dependence of R_g^2 on M for PS in A1248 with $10^4 \leq M \leq 10^5$ is very well described by $Nb^2/6$, the BSM prediction, provided that b is chosen as 5.0 nm.[13,25] This value is smaller than that extracted from the chain dynamics measurements. The possible significance of this difference is not immediately clear. On the one hand, perhaps a factor of 20% in b should not be viewed as a serious discrepancy. Alternatively, the difference might reflect a breakdown of the BSM that is not apparent in the analyses of the dynamic quantities, which appear to be internally consistent. The magnitude of b, corresponding to a subchain containing approximately 50 monomers, is much larger than the static persistance length of PS. The value of M_s (and ultimately b) extracted from the OFB results hinges directly on the surprising appearance of a distinct end to the relaxation spectrum at a relatively long time and length scale. The resolution of this issue might well result in significantly modified parameter values. Another possibility is that incorporation of excluded volume in the BSM, by one of several approximate schemes, would change the parameter values. Lastly, as noted previously,[25] the fact that R_g scales with $M^{0.5}$ for $M < 10^5$ for this system is somewhat surprising, given that A1248 is a moderately good solvent for PS. However, the diffusion data in Figure 16 indicate that solvent quality plays only a small role for $M < 10^5$. With the imminent development of superior neutron scattering facilities at the NIST, we intend to pursue measurements of R_g for higher molecular weight PS, which should provide more opportunity to investigate this point further.

Various nondimensional groups can be formed from the measured properties discussed in this report. An example is presented in Figure 18, where the ratio $D_0\tau_1^\circ/R_g^2$ is plotted as a function of M. In this case, the actual D_0 and τ_1° values were used for all five points, except for the largest M point where an interpolated value of τ_1° was employed; the infinite dilution R_g values were determined either by interpolation (highest two M) or by extrapolation (lowest three M). The error bars indicate relative uncertainties of ±10% in each measured quantity. The smooth curve represents the BSM prediction with $M_s = 5 \times 10^3$ and $h^* = 0.15$. However, the sensitivity to h^* is very weak, particularly in the plateau attained at large M. The BSM is within ≃25% of a quantitative prediction for this ratio, which is formed from the results of four completely different experimental techniques; this conclusion is insensitive to the choice of parameter values. The fact that the data lie above the theoretical curve is directly related to the appearance of R_g in the denominator, and the previously noted lower value of b (i.e., if R_g were also described by b = 6.0 nm, then the data and theory in Figure 18 would match almost exactly).

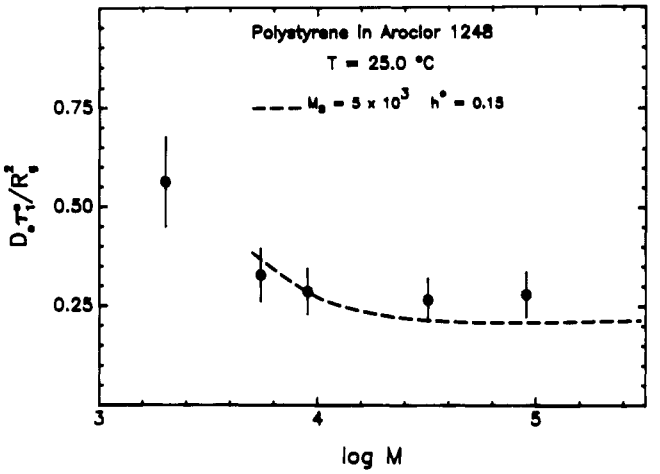

Figure 18. Dimensionless quantity $D_0\tau_1^\circ/R_g^2$ versus molecular weight for PS in A1248 at 25.0 °C, compared with the predictions of the BSM.

Summary

The technique of oscillatory flow birefringence has been used to determine the infinite dilution conformational dynamics properties of four low molecular weight polystyrenes (2×10^3, 5.5×10^3, 2.0×10^4, and 3.2×10^4) in Aroclor 1248 (A1248). The techniques of field-gradient NMR and forced Rayleigh scattering have been used to determine the infinite dilution diffusivities for five low and moderate molecular weight PS (2.0×10^3, 5.5×10^3, 9.0×10^3, 3.2×10^4, and 9.0×10^5) in A1248. These results have been combined with intrinsic viscosities and radii of gyration from the literature for the same system and the same M range and interpreted in the framework of the bead–spring model. The principal conclusions from this work are as follows.

1. With one choice of values for the three BSM parameters, it is possible to describe the experimentally observed relaxation spectrum, longest relaxation time, diffusivity, and intrinsic viscosity, in a quantitative fashion. This success is predicated on the correct subtraction of the solvent contribution to the measured solution properties.

2. This success of the BSM, with its crude description of the dynamics of a polymer chain on a local scale, is somewhat surprising, as it apparently persists down to values of M corresponding to a single bead–spring unit.

3. The most intriguing result is the fact that the OFB results indicate a well-defined short time end to the relaxation spectrum, corresponding to a single bead–spring unit containing approximately 50 monomers. This observation has been made previously and is equally evident in viscoelastic measurements on the same system. While it is clear that conformational rearrangements must occur on shorter length scales, they are not evident in these measurements.

4. The exact values of the BSM parameters employed here should not be viewed as definitive, for several reasons. First, when the phenomenon identified in point 3 is explained, reevaluation of the significance of the parameters will undoubtedly be appropriate. Second, inclusion of excluded volume in the BSM can also change the parameter values; for example, the effects of excluded volume on the relaxation spectrum, here modeled by varying h^*, can be equally well accounted for with an

approximate excluded volume term. In particular, the use of an intermediate value of h^* to describe the results presented here does not necessarily indicate that the chains are "partially draining".[47]

Acknowledgment. This work was supported by the National Science Foundation through Grants DMR-8319291 and DMR-8715391, and by the University of Minnesota NSF-ERC Center for Interfacial Engineering. Helpful discussions with J. L. Schrag are gratefully acknowledged.

References and Notes

(1) Ferry, J. D. *Viscoelastic Properties of Polymers*, 3rd ed.; Wiley: New York, 1980, and references therein.
(2) Miller, J. W.; Schrag, J. L. *Macromolecules* **1975**, *8*, 361.
(3) Brueggeman, B. G.; Minnick, M. G.; Schrag, J. L. *Macromolecules* **1978**, *11*, 119.
(4) Lodge, T. P.; Miller, J. W.; Schrag, J. L. *J. Polym. Sci., Polym. Phys. Ed.* **1982**, *20*, 1409.
(5) Lodge, T. P.; Schrag, J. L. *Macromolecules* **1982**, *15*, 1376.
(6) Martel, C. J. T.; Lodge, T. P.; Dibbs, M. G.; Stokich, T. M., Jr.; Sammler, R. L.; Carriere, C. J.; Schrag, J. L. *Faraday Symp. Chem. Soc.* **1983**, *18*, 173.
(7) Lodge, T. P.; Schrag, J. L. *Macromolecules* **1984**, *17*, 352.
(8) Landry, C. J. T. Ph.D. Thesis, University of Wisconsin, 1985.
(9) Radtke, D. R. Ph.D. Thesis, University of Wisconsin, 1986.
(10) Merchak, P. A. Ph.D. Thesis, University of Wisconsin, 1987.
(11) Stokich, T. M., Jr. Ph.D. Thesis, University of Wisconsin, 1988.
(12) Strand, D. A. Ph.D. Thesis, University of Wisconsin, 1989.
(13) Amelar, S. Ph.D. Thesis, University of Minnesota, 1989.
(14) Sammler, R. L.; Landry, C. J. T.; Woltman, G. R.; Schrag, J. L. *Macromolecules* **1990**, *23*, 2388.
(15) Hermann, K. C. Ph.D. Thesis, University of Minnesota, 1990.
(16) Schrag, J. L.; Stokich, T. M.; Strand, D. A.; Merchak, P. A.; Landry, C. J. T.; Radtke, D. R.; Man, V. F.; Lodge, T. P.; Morris, R. L.; Hermann, K. C.; Amelar, S.; Eastman, C. E.; Smeltzly, M. A. *J. Non-Cryst. Solids*, in press.
(17) Zimm, B. H.; Kilb, R. W. *J. Polym. Sci.* **1959**, *37*, 19.
(18) Soli, A. L.; Schrag, J. L. *Macromolecules* **1979**, *12*, 1159.
(19) Dibbs, M. G. Ph.D. Thesis, University of Wisconsin, 1983.
(20) Sammler, R. L.; Schrag, J. L. *Macromolecules* **1988**, *21*, 1132; 3273.
(21) Wang, F. W. *Macromolecules* **1975**, *8*, 364; **1978**, *11*, 1198.
(22) Man, V. F. Ph.D. Thesis, University of Wisconsin, 1984. Soli, A. L. Ph.D. Thesis, University of Wisconsin, 1978.
(23) Man, V. F.; Schrag, J. L.; Lodge, T. P. *Macromolecules*, in press.
(24) Rouse, P. E., Jr. *J. Chem. Phys.* **1953**, *21*, 1872. Zimm, B. H. *J. Chem. Phys.* **1956**, *24*, 269.
(25) Lodge, T. P.; Hermann, K. C.; Landry, M. R. *Macromolecules* **1986**, *19*, 1996.
(26) Thurston, G. B.; Schrag, J. L. *J. Polym. Sci., Polym. Phys. Ed.* **1968**, *6*, 1331.
(27) Kim, H.; Chang, T.; Yohanan, J. M.; Wang, L.; Yu, H. *Macromolecules* **1986**, *19*, 2737.
(28) Morris, R. L.; Lodge, T. P. *Anal. Chim. Acta* **1986**, *189*, 183.
(29) Amis, E. J.; Carriere, C. J.; Nestler, F. H. M.; Schrag, J. L.; Ferry, J. D. *Anal. Chim. Acta* **1986**, *189*, 199.
(30) von Meerwall, E. D.; Amelar, S.; Smeltzly, M. A.; Lodge, T. P. *Macromolecules* **1989**, *22*, 295, and references therein.
(31) Huang, W. J.; Frick, T. S.; Landry, M. R.; Lee, J. A.; Lodge, T. P.; Tirrell, M. *AIChE J.* **1987**, *33*, 573.
(32) Janeschitz-Kriegl, H. *Adv. Polym. Sci.* **1969**, *6*, 170. *Polymer Melt Rheology and Flow Birefringence*, Springer-Verlag: Berlin, Germany, 1983.
(33) Fuller discussions of the phenomenology of η'_∞ and S'_∞ are available in refs 3, 7–13, and 34.
(34) Morris, R. L.; Amelar, S.; Lodge, T. P. *J. Chem. Phys.* **1988**, *89*, 6523.
(35) Muthukumar, M.; Freed, K. F. *Macromolecules* **1978**, *11*, 5.
(36) Kirkwood, J. G.; Riseman, J. *J. Chem. Phys.* **1948**, *16*, 565.
(37) Thurston, G. B.; Peterlin, A. *J. Chem. Phys.* **1967**, *46*, 4881.
(38) See, for example: Hair, D. W.; Amis, E. J. *Macromolecules* **1990**, *23*, 1889, and references therein.
(39) Lodge, A. S.; Wu, Y.-J. *Rheol. Acta* **1971**, *10*, 539.
(40) Freed, K. F.; Edwards, S. F. *J. Chem. Phys.* **1974**, *61*, 3626; 4032; *J. Chem. Soc. Trans.* **1975**, *171*, 1.
(41) Freed, K. F.; Perico, A. *Faraday Symp. Chem. Soc.* **1983**, *18*, 29.
(42) Muthukumar, M. *J. Chem. Phys.* **1983**, *79*, 8.
(43) Adler, R. S.; Freed, K. F. *Macromolecules* **1978**, *11*, 1058.
(44) Huber, K.; Bantle, S.; Lutz, P.; Burchard, W. *Macromolecules* **1985**, *18*, 1461.
(45) Yamakawa, H.; Fujii, M. *Macromolecules* **1973**, *6*, 407.
(46) Yamakawa, H. *Modern Theory of Polymer Solutions*; Harper and Row: New York, 1971.
(47) Oono, Y. *Adv. Chem. Phys.* **1985**, *61*, 301.